The Meteoritical Society

Meteoritics & Planetary Science 56, Nr 6, 1073–1085 (2021)
doi: 10.1111/maps.13663

Recovery of meteorites using an autonomous drone and machine learning

Robert I. CITRON[1]*, Peter JENNISKENS[2,3], Christopher WATKINS[4], Sravanthi SINHA[5], Amar SHAH[6], Chedy RAISSI[7], Hadrien DEVILLEPOIX[8], and Jim ALBERS[2]

[1]Department of Earth and Planetary Sciences, University of California, Davis, Davis, California 95616, USA
[2]SETI Institute, Mountain View, California 94043, USA
[3]NASA Ames Research Center, Moffett Field, California 94035, USA
[4]Scientific Computing, Commonwealth Scientific and Industrial Research Organisation, Clayton, Victoria 3181, Australia
[5]Holberton School of Software Engineering, San Francisco, California 94111, USA
[6]Department of Engineering, Computational and Biological Learning, Cambridge University, Cambridge CB2 1PZ, UK
[7]Institut National de Recherche en Informatique et en Automatique, Villers-lès-Nancy 54506, France
[8]Space Science & Technology Centre, School of Earth and Planetary Sciences, Curtin University, GPO Box U1987, Perth, Western Australia 6845, Australia
*Corresponding author. E-mail: rcitron@ucdavis.edu

(Received 01 October 2020; revision accepted 25 April 2021)

Abstract–The recovery of freshly fallen meteorites from tracked and triangulated meteors is critical to determining their source asteroid families. Even though our ability to locate meteorite falls continues to improve, the recovery of meteorites remains a challenge due to large search areas with terrain and vegetation obscuration. To improve the efficiency of meteorite recovery, we have tested the hypothesis that meteorites can be located using machine learning techniques and an autonomous drone. To locate meteorites autonomously, a quadcopter drone first conducts a grid survey acquiring top-down images of the strewn field from a low altitude. The drone-acquired images are then analyzed using a machine learning classifier to identify meteorite candidates for follow-up examination. Here, we describe a proof-of-concept meteorite classifier that deploys off-line a combination of different convolution neural networks to recognize meteorites from images taken by drones in the field. The system was implemented in a conceptual drone setup and tested in the suspected strewn field of a recent meteorite fall near Walker Lake, Nevada.

INTRODUCTION

In order to better understand the early evolution of the solar system, there is an ongoing effort to determine the composition of some 40 asteroid families in the asteroid belt. Remote sensing information is complemented with data gleaned from laboratory studies of meteorites. To put that meteoritic data in context, the approach orbit of freshly fallen meteorites is measured to determine which asteroid family might have produced the meteoritic debris from a particular collision event. This is a statistical effort to determine the inclination and semimajor axis distribution of the approach orbits of meteorites of the same type with the same collision age. The inclination identifies the inclination of the source region, while the semimajor axis points to the delivery resonance (Jenniskens 2013, 2018).

If the meteorite can be recovered, the corresponding fireball's light curve and deceleration profile also provide information regarding the deposition of the meteoroid's kinetic energy into the Earth's atmosphere, which is a function of the meteoroid's density and internal strength. That information can be used to improve predictions of the altitude where various types of meteors fragment, which is critical to understanding events that lead to damaging airbursts (Popova et al. 2013).

Building a statistical database of asteroid family compositions requires a large number of meteorites with known trajectories to be located in the field. Yet so far, in only 40 cases have meteorites been recovered from observed falls in which the fireball trajectory was measured sufficiently to determine the pre-impact orbit (Jenniskens 2013; Borovička et al. 2015). In many of

these cases, the fireball data were obtained from serendipitous security or dash-cam footage, resulting in a less accurate estimate of the pre-impact orbit. The most accurate fireball trajectories are measured using dedicated all-sky camera networks. However, although fireball networks have published approximately 800 meteoroid trajectories significant enough to have dropped meteorites on the ground, so far, only ~36 cases have resulted in meteorite recovery, and only 21 cases (3%) were recovered in dedicated networks (Jenniskens 2013; Borovička et al. 2015; Gardiol et al. 2020).

The low percentage of observed falls that result in meteorite recovery is due to the extreme difficulty in recovering meteorites. Meteorites are typically scattered over large strewn fields (many square kilometers) and found through a physical survey that typically requires ~100 man-hours to locate one meteorite fragment. The investment of that time is made more often when the falling meteorites are detected by Doppler weather radar, which provides confidence that meteorite fragments fell within a particular search area (e.g., Jenniskens et al. 2012). Large-scale searches are also generally conducted for only the largest falls, even though all-sky networks detect many smaller fireballs that may have deposited fragments on the ground.

In order to increase the recovery yield of the more frequent smaller falls, a more efficient method of searching for freshly fallen meteorites is required. One possibility is autonomous meteorite localization using a drone survey coupled with a machine learning object detection algorithm. An autonomous quadcopter drone can navigate terrain at a fixed height, obtaining a survey of top-down images. These images can be spliced and fed into a machine learning object detection classifier, which can determine the location of potential meteorites in each image. If successful, the combination of automated drone surveys and machine learning object detection could reduce the man-hours needed to locate freshly fallen meteorites and increase the likelihood of locating meteorites in strewn fields.

Prior Work

The use of drone surveys to locate freshly fallen meteorites has gained increasing traction in recent years (Citron et al. 2017; Zender et al. 2018; Alowais et al. 2019; Anderson et al. 2020). The general method of autonomous meteorite detection using drones involves applying a machine learning classifier to images acquired from a low-altitude survey (Citron et al. 2017). The drone first surveys the field obtaining top-down images of the search area. With a sufficient field of view and image resolution, each 1–3 cm meteorite fragment should be resolved by >20 pixels in width, sufficient for image classification. A trained machine learning classifier is then used to identify any potential meteorites in each image.

Training a machine learning classifier to detect freshly fallen meteorites presents a challenge. The main identifying characteristic of a meteorite fragment is that it should appear to not belong in the surrounding terrain. Although freshly fallen meteorites should appear quite distinct from native rocks, meteorites are diverse and it is impossible to know the characteristics of the next freshly fallen meteorites or the surrounding terrain. While meteorites typically are darker than native rocks due to the fusion crust obtained during atmospheric entry, some meteorites lack a fusion crust because of subsequent breakup. Meteorites are also only sparsely distributed throughout the strewn field, with search areas up to several square kilometers potentially containing only a few meteorites 1–3 cm in size. A machine learning classifier therefore must return sufficiently low false-positive detections to make a square kilometer survey feasible, while also being versatile enough to detect meteorites of a variety of types on completely new terrains.

The construction of a machine learning classifier to identify meteorites in various terrains has been explored by several groups (Citron et al. 2017; Alowais et al. 2019; Anderson et al. 2019, 2020). The most suitable machine learning classifiers for meteorite identification are based on convolutional neural networks (LeCun et al. 1998), which have achieved state-of-the-art performance in a variety of computer vision-based tasks (Gu et al. 2018). Classifiers based on convolution neural networks avoid problems associated with hand picking features, which would be inadequate for meteorite identification because of the diverse properties of meteorites. The key benefit of a neural network-based classifier is that it is trained to learn the features most relevant for its task jointly with the output predictions it makes. Thus, a general classifier can be constructed using deep learning algorithms to locate freshly fallen meteorites on most terrains.

There are two main types of machine learning models applied to object recognition: binary image classifiers or object detection networks. A binary image classifier analyzes an entire image and determines what object it represents. Binary image classifiers are trained on sets of "positive" and "negative" images, and when a trained binary classification network is applied to a new image, it determines the likelihood the image falls in the "positive" or "negative" category (i.e., if the image is of a meteorite or not). For a binary classifier to work, the meteorite must encompass most of the image, meaning that a large image acquired by a drone must be spliced

into multiple smaller image patches before being analyzed by the classifier (Citron et al. 2017). Alternatively, object detection networks are trained on sets of larger images where each object class is demarcated (usually by a box) within each training image. The object detection network learns to identify zones within an image where potential objects of each class may be located. When a trained object detection network is applied to a new image, it outputs a box around each section of the image where it predicts an object class is located. Each zone with a potential object detection is given a model score based on the likelihood it represents the desired object. Object detection networks can be fed an image of any size and locate multiple objects within the image. This is more time efficient because each drone-acquired image does not need to be spliced into smaller fragments that must be classified independently.

Several studies have tested the use of a machine learning classifier to find freshly fallen meteorites in the field. An earlier version of our system was tested in Creston, California (Citron et al. 2017); however, that iteration used a binary image classifier that required each image to be spliced into ~64 × 64 pixel patches before classification. This resulted in long processing times for each full image. Our binary classifier also returned many false positives on certain terrain types. Zender et al. (2018) also tested meteorite detection using a drone-mounted camera, but did not use a machine learning classifier and instead applied a simple algorithm based on reflectance characteristics. Alowais et al. (2019) performed real-time detection of meteorites by implementing a machine learning algorithm on board a drone. Their algorithm processed images from a live video feed and achieved an accuracy of ~90%. Anderson et al. (2020) implemented the Keras machine learning module applied to 200 × 200 pixel tiles spliced from drone-acquired images. They constructed a training data set by pasting meteorite images into drone-acquired images of the local terrain and trained a binary image classifier to identify meteorites with validation accuracy of ~97%. In a field test, Anderson et al. (2020) surveyed a strewn field using an RGB camera mounted on a multicopter drone, covering ~1 km^2 per day at a resolution of 1.8 mm per pixel. Their machine learning approach was able to correctly identify three real meteorites (two falls, one find) in their native fall locations.

Machine learning is a rapidly advancing field and new tools continually increase the accuracy of object detection and classification. Of particular interest are residual neural networks that have achieved excellent performance in visual recognition tasks (He et al. 2016). The residual learning framework can be used to train deeper neural networks capable of advanced object detection independent of the image size. Thus, instead of training a binary image classifier to examine many small patches (<200 pixels in width; e.g., Citron et al. 2017; Anderson et al. 2020), an effective object detection network can be trained to recognize small meteorites in full images. Utilizing these recent advances, we trained a residual neural network-based object detection network to recognize meteorites in drone-acquired images and test its accuracy in the field.

Here, as a proof of concept, we constructed an object detection network using images of meteorites collected from an autonomous drone. We chose an inexpensive off-the-shelf drone model (3DR) and camera (GoPro Hero4) in hope that our algorithm could later be applied on a much bigger scale by owners of such equipment. We show that classification of meteorites in drone images is possible, and tested our model at the location of a recent suspected strewn field in Walker Lake, Nevada.

METHODS

Constructing the Machine Learning Classifier

Training Data Set

Any machine learning classifier requires a large training data set of thousands of positive and negative images. Because a future meteorite fall could involve any type of meteorite fragment and terrain type, we constructed a data set containing a variety of meteorite types on a diverse set of terrains. A classifier trained on such an image set could be readily applied to the classification of images from a future fresh meteorite fall. We used three sources for meteorite images to construct a large training data set: (1) placing a limited collection of eight meteorites in our possession on various local terrains and taking overhead images of them, (2) placing our collection of eight meteorites in a recent meteorite strewn field and imaging them from above with a drone, and (3) using overhead shots of freshly fallen meteorites obtained from a search of publicly available internet resources.

For collecting images of meteorites on local terrains, we used our collection of eight meteorites 10–100 g in mass (1–4 cm in diameter) obtained fresh from the 1992 Mbale meteorite fall (Jenniskens et al. 1994). The meteorites were deployed on various local grass, dirt, sand, and rocky terrains, and imaged with smart phone cameras and a DSLR from above at a similar height as the expected drone images. Each image was spliced into smaller patches of 1000 × 600 pixels. Although the object detection network described in the Training the Object Detection Network section can

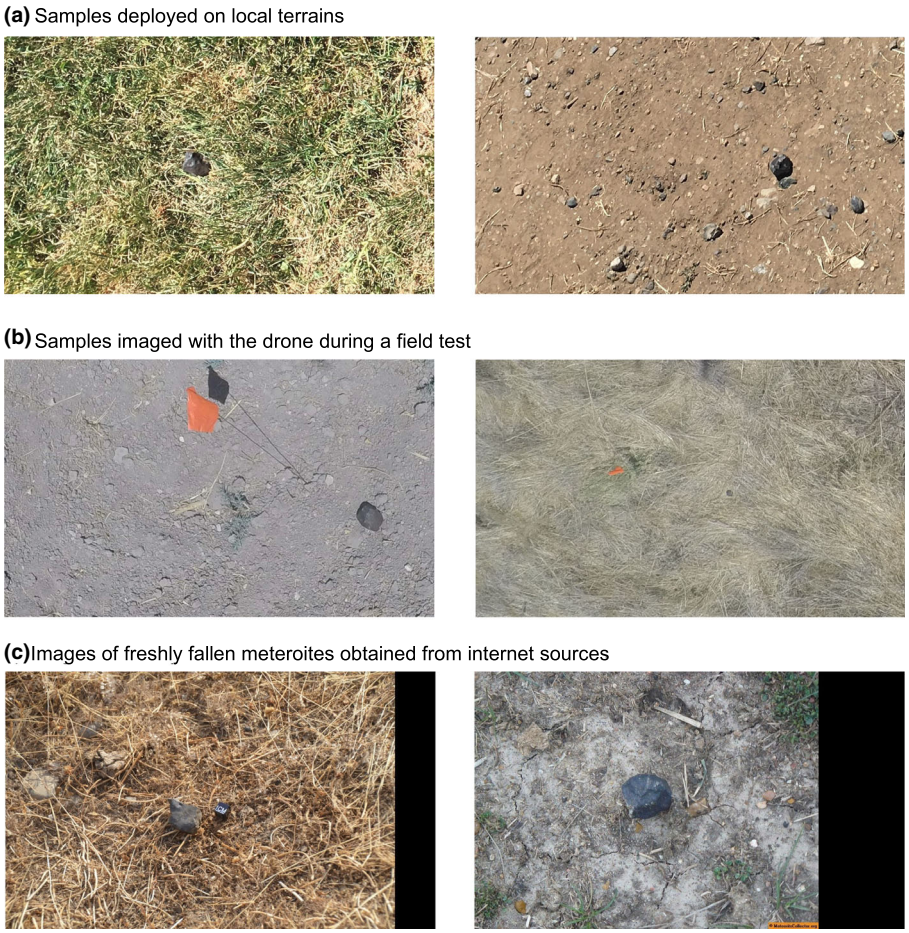

Fig. 1. Examples of images used to train our object detection data set. a) Images of two meteorites from our collection placed on local terrains and captured from above with a DSLR camera. b) Images of two meteorites from our collection captured during a field test in Creston, California, with a GoPro Hero4 camera mounted on a 3DR Solo Drone. c) Example images of freshly fallen meteorites obtained from publicly available internet resources. (Color figure can be viewed at wileyonlinelibrary.com.)

work on images of any size, we found that processing was limited by computer memory requirements during image classification and 1000 × 600 pixel image patches resulted in good performance. Examples of image patches containing meteorites are shown in Fig. 1a. We used 526 such image patches in the training data set.

The second source of test images was from a previous test of an earlier iteration of our machine learning classifier. During this prior test, we deployed our eight meteorites in the location of a recent meteorite fall near Creston, California, and imaged the fragments from above with a drone-mounted camera (Citron et al. 2017). For the updated object detection classifier described in this paper, we used the images from our previous test as an additional data source of training data. Because these images were taken with the same camera and drone system, they are more applicable to future field deployments and of high value to training our updated model. Each image was spliced into smaller 1000 × 600 pixel image patches before being added to the training data set. Example training data from our field test are shown in Fig. 1b. We used 82 image patches obtained from the drone-mounted camera during our field test in Creston, California.

The third source of training images was obtained from an internet search for pictures of freshly fallen meteorites. Images of meteorites obtained from internet resources were critical because we did not want to overtrain our object detection network on the eight meteorites in our collection. Including images of meteorites from various falls worldwide in our data set allowed us to train our model on a variety of different meteorite types and background terrains, enhancing our ability to deploy our machine learning algorithm at the site of a future fresh fall. Each meteorite image obtained from the internet search was re-scaled or cropped to 1000 × 600 pixels, so the training data set contained similar image sizes. Overall,

we included 155 meteorite images collected from the internet in our data set. Example images of meteorites obtained from the internet search are shown in Fig. 1c.

Overall, our training data set contained 526 images of our eight fragments placed on local terrains, 82 images of our eight fragments taken during a field test, and 154 images of meteorites obtained from the internet search. These image sources were combined into a single data set of 762 images. The training data set was separated into a training and validation subset. The validation subset was 150 images randomly selected images (~20% of the full data set) and the training subset was the remaining 612 images. Because the number of meteorite images in our data set was limited, we augmented the training data set by reflecting each image across the horizontal plane, vertical plane, and both the horizontal and vertical planes, resulting in a total of 2448 images in the training data set.

Training the Object Detection Network

For meteorite detection, we used the RetinaNet object detection network (Lin et al. 2017). RetinaNet is a highly efficient object detection network built upon the ResNet deep residual neural network architecture (He et al. 2016). The implementation of RetinaNet utilizes the Keras (Chollet 2015), Caffe (Jia et al. 2014), and Tensorflow (Abadi et al. 2015) software packages. We used the ResNet-50 backend (He et al. 2016), which is pretrained using a data set of roughly 15 million images called ImageNet (Russakovsky et al. 2015). This approach means that from initializing our training phase, the object detection network would already be familiar with objects such as grass, rocks, hay, etc., and would not have to learn their features from scratch. We took the pretrained model and trained it on our data set of meteorite images for several epochs with RetinaNet in order to obtain a final object detection model. We trained the model for three epochs until the classification loss was <0.05 to obtain high accuracy without over-fitting our training data.

Once trained, RetinaNet could process a 1000 × 600 pixel image in 135−146 ms on our field laptop equipped with an NVIDIA GeForce GTX 980 graphics card. Each image taken with the drone-mounted GoPro camera was 4000 × 3000 pixels (12 Mp) and was spliced into 47 1000 × 600 pixel patches using a 200 pixel spacing to avoid splitting any potential meteorites across image patches. This resulted in a total processing time of 6.6 s for each full GoPro image. In our field test (see the Field Test and Results section), each 20–25 min flight acquired an average of 200 images, for a processing time of 22 min per flight. A day's worth of data (10–15 flights) could therefore be processed in 4–6 h.

While RetinaNet obtained a low classification loss, field deployment inevitably involves many false-positive identifications because many terrain types contain dark rocks that might be mistaken for meteorites. It is important to emphasize that the goal of the object detection network is not to return only a few images of suspected meteorites with 100% accuracy, but instead return 100s of candidate image patches that might contain a meteorite fragment within a given search area. As long as the number of candidate patches is manageable (hundreds of images and not tens of thousands), the user can scan through the image patches and flag particularly strong candidates for follow-up examination.

Drone Hardware and Field Deployment

In our deployment, we used the 3DR Solo quadcopter drone fitted with a gimbal-mounted GoPro HERO 4 camera. Because of the hilly terrain in much of California, we upgraded the 3DR Solo drone with a laser altimeter and the PixHawk GreenCube flight controller capable of running Arducopter 3.4. This allowed the drone to use true terrain following to maintain a constant elevation above the ground. We upgraded the GoPro with a narrow-angle lens offering an 87 degree field of view. Flying at a height of 3 m with the 4000 × 3000 pixel GoPro camera yields a resolution of 0.97 mm per pixel. At 6 m, the resolution is 1.95 mm per pixel. To obtain the desired resolution of ~20 pixels across a meteorite fragment, the drone was flown at 3 m when searching for smaller fragments ~2 cm across (10–20 g) and 6 m when searching for larger fragments >4 cm across (75–150 g).

Each drone survey was programmed with the Mission Planner software, which allowed us to prefetch the map data prior to field deployment. During field deployment, we programmed the drone to fly a grid-search pattern and take photos from a constant altitude of 2−6 m. The battery limited ~25 min flight time of the 3DR Solo drone resulted in ~130–250 images per survey, depending on the flight altitude and search pattern. Because our object detection classifier identifies many false meteorite candidates, the user must scan through the processed images to determine which candidates are worth follow-up examination during a future field visit. Each image is tagged with a timestamp that can be compared to the drone's GPS log to determine the approximate location where the image was acquired. Although in principle it is possible to process the images and scan for candidates in the field, we found this was more easily accomplished out of the field. During field deployment, we acquired images for a full day and processed the images during the evening.

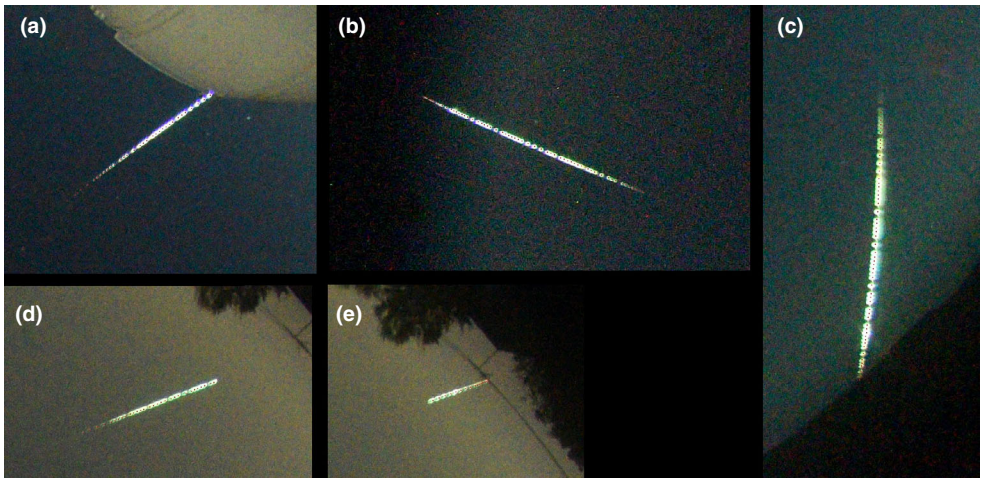

Fig. 2. NASA Meteorite Tracking and Recovery Network imaging of July 14, 2019 bolide from (a) Lick Observatory, (b) Mount Umunhum, (c) Alan Telescope Array, (d) Sunnyvale—early part of the bolide, and (e) Sunnyvale—late part of the bolide. (Color figure can be viewed at wileyonlinelibrary.com.)

We then examined the processed images and flagged potential meteorite candidates for follow-up during a second trip to the field site the next day.

FIELD TEST AND RESULTS

Potential Meteorite Fall at Walker Lake, Nevada

On July 14, 2019, at 09:36:50 UTC, a bright meteor of 4.1 s duration was captured by four stations of the NASA Meteorite Tracking and Recovery Network, part of the Global Fireball Observatory. The fireball track was detected from stations at Lick Observatory, Mt. Umunhum, Sunnyvale, and the Allen Telescope Array (Fig. 2). The images were calibrated and the meteor track extracted (Devillepoix et al. 2020). The beginning height of the meteor was at 82.054 km and the end height was at 27.066 km over the Sierra Nevada mountains. The approach orbit was asteroidal, with $a = 2.358 \pm 0.032$ AU and $i = 10.72 \pm 0.08°$. The entry speed was relatively high at 21.937 ± 0.114 km s^{-1}, but the surviving mass was calculated to be as much as 35.3 ± 3.7 kg (EKS model; Devillepoix et al. 2020). The meteor had a 41° slope with lateral uncertainty in the trajectory of order 250 m due to a relatively large minimum distance of 275 km between the meteor and the stations.

Analysis of the wind drift during the dark flight calculations was done using the Oakland Wind sonde data before and after the time of fall, using the software WIND with an assumed density of 3.2 g cm^{-3} (Jenniskens et al. 2019). This resulted in expected fragments of 1 g, 10 g, 100 g, and 1 kg located near Walker Lake, Nevada within the Walker River Indian Reservation of the Walker River Paiute Tribe, headquartered at Schurz, Nevada. The expected strewn field location is shown in Fig. 3. Solutions were calculated with descent starting from both the final flare (white markers) and the final observed point of the trajectory (blue). In the latter case, winds would have blown small meteorites toward the larger ones, shortening the strewn field. The area is a former lake bed of Walker Lake and has sand dunes and stretches of rock-strewn flat areas. The vegetation is minimal, but increases in density toward the river.

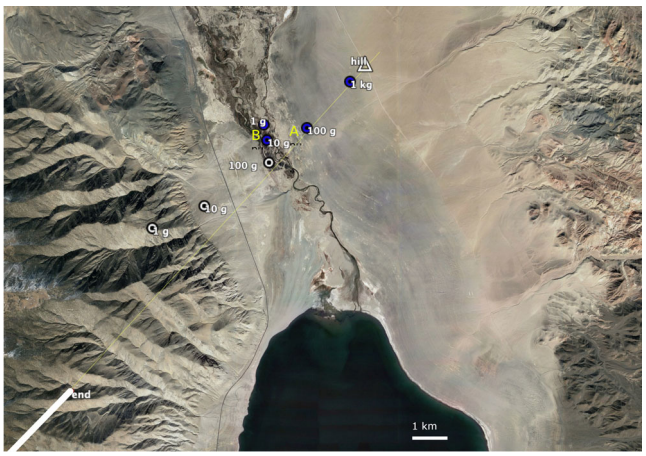

Fig. 3. Map of the expected Walker Lake strewn field. The white line indicates the final part of the meteor trajectory based on NASA Meteorite Tracking and Recovery imagery. The yellow line is an extension. The dots mark the anticipated location for meteorites falling from the final flare (white markers) and the end point (blue markers), based on Oakland wind sonde data and the WIND dark flight model. Sites A and B are marked with yellow text. (Color figure can be viewed at wileyonlinelibrary.com.)

Table 1. Field test runs.

Test	Site	Altitude (m)	Images	Total patches	Positives	Negatives
1	A	2	256	12,240	3553	8687
2	A	2	245	11,232	2322	8910
3	A	2	288	13,824	1328	12,496
4	A	3	145	6960	679	6281
5	B	3	135	6480	2019	4461
6	B	3	129	6192	2769	3423
7	B	6	214	10,272	2377	7895
8	B	6	175	8400	875	7525
9	B	6	190	9120	399	8721
10	B	6	225	10,800	800	10,000

Field Test

We received permission from the Walker River Northern Paiute Tribe to conduct a field test of our meteorite classification system in Walker Lake, Nevada, the site of a meteorite fall on July 14, 2019 (Fig. 3). Overall, we conducted 10 test flights at two different sites within the expected strewn field. Site A was near the 10 g marker in Fig. 3, where we expected 1–20 g fragments. Site B was near the 100 g marker in Fig. 3, where we expected 50–150 g fragments. Due to the smaller expected fragment size at Site A, we flew the drone at a lower altitude (2–3 m). At Site A, we also deployed our collection of eight meteorites during each test flight to confirm our ability to detect the meteorites used to train our classifier on a new terrain type. At Site B, we conducted higher altitude (3–6 m) surveys to cover a larger area and potentially find a single large fragment ~100 g.

A summary of the 10 test flights and results is shown in Table 1. Four tests were conducted at Site A, three at 2 m and one at 3 m. Six tests flights were conducted at Site B, two at 3 m and four at 6 m. During each test flight, the drone acquired images for ~20 min, limited by the battery life of the drone. Each test flight acquired 129–288 full GoPro images. These full 4000 × 3000 pixel images were spliced into overlapping image patches of 1000 × 600 pixels. The image patches were analyzed with the trained RetinaNet model. An image patch was classified as "positive" if it contained an object classified as a meteorite with a score of 0.5 or higher, and all other image patches were classified as "negative." The number of positive and negative image patches is listed in Table 1. Each test flight resulted in a large number of image patches classified as positive. This was particularly true for the low-altitude flights, where there were on average ~2650 positive patches per test flight (~28% of all patches). This is mostly due to the large number of other rocks in the survey area, and illustrates the difficulty of locating meteorites remotely on rocky terrain. The higher altitude flights (6 m) resulted in less positive patches, with an average of ~1112 positive patches per test flight (~12% of the all patches). Test flight 5 contained around three times as many positive patches as the other 6 m flights, which was likely due to the rockier terrain in the test flight 5 path.

The results in Table 1 show that RetinaNet returns a large number of false positives for a given search area. For the 2–3 m test flights, the number of positive patches returned was prohibitive, meaning that the thousands of positive patches flagged for follow-up is too cumbersome to sort through and identify expected meteorites. For the 6 m test flights, the number of positive patches was sufficiently low to allow a user to quickly scan through the positive image patches and identify fragments for follow-up with an additional field visit.

Apart from generally determining the number of positive patches during field surveys, we conducted two critical tests to determine the feasibility of using our system in the field. The first test was to deploy our collection of known meteorites in the drone survey path and assess the ability of our machine learning algorithm to correctly identify these fragments on novel terrain. The second test was to scan through the most likely meteorite candidates flagged by our trained RetinaNet model and attempt to relocate them in the field. For this test, we determined the geolocation of each meteorite candidate by cross-referencing the image timestamp with the drone GPS log.

The test of our ability to correctly identify known meteorites on novel terrain was conducted at Site A, where we deployed several of the eight meteorite samples in our collection in the drone flight path during each drone survey. An example image from such a test is shown in Fig. 4. As described in the Methods section, each full GoPro image was split into smaller 1000 × 600 pixel patches that were then analyzed with the object detection model. Examples of image patches containing correctly identified meteorites and false positives are shown in Fig. 5. The two meteorites from Fig. 4 were correctly identified in the smaller image patches and given a model score of 1.0 by the object detection algorithm (Fig. 5a). Several false positives were also identified with two examples shown in Fig. 5b, which were given scores of 0.89 and 0.76. Overall, of the four low-altitude test flights where we deployed meteorites in the survey path, our object detection model correctly located all of the deployed meteorites with corresponding model scores of 0.97–1. This is not surprising because the meteorites we deployed in the field were the same meteorites used to

Fig. 4. Example image of two test meteorites placed in terrain new to the machine learning algorithm, during a field test near Walker Lake, Nevada. The meteorites are marked with orange flags. (Color figure can be viewed at wileyonlinelibrary.com.)

train our model. However, we did deploy the meteorites on completely new terrain that was used during the model training, illustrating the ability of our object detection network to locate our meteorite samples on a new terrain not used in the training data.

The test of our ability to locate candidate meteorite flagged by our object detection algorithm in the field was conducted at Site B, where we scanned through the positive image patches from the higher altitude (6 m) surveys. We identified three meteorite candidates that we attempted to locate in the field. The three drone images flagged for follow-up are shown in Figs. 6 and S1 and S2 in supporting information. The GPS coordinates of the three meteorite candidates were referenced to the drone flight log to determine the expected GPS coordinates where the images were acquired. During the second trip to the field the day after the flight tests, we visited the expected GPS coordinates of each of the three candidate meteorites. Using the drone images as a reference, we successfully located all three meteorite candidates. Close-up images of the three meteorite candidates located in the field are shown in Fig. 7. Only two of the three stones we had flagged appeared a good meteorite candidate upon closer in situ examination (Figs. 7a and 7b). These two meteorites were dark rocks, similar in appearance to meteorites. The candidate that was not a good match to a meteorite fragment (Fig. 7c, corresponding to Fig. S2) was on closer examination a patch of dark brush combined with a shadow. This illustrates that in some cases, shadows, poor resolution, and camera perspective can confuse the identification of meteorite candidates. Still, two candidates showed a good match to what might be expected from a fresh meteorite fall and were able to be located in the field after georeferencing the flagged images. As a proof of concept, this illustrated the ability of our method to locate meteorite candidates in the field which were previously flagged in images acquired from prior surveys.

DISCUSSION

Our field deployment highlighted several areas of improvement required to make drone searches for meteorites more effective. The primary area of improvement is the object detection classifier. Because our local collection of meteor fragments was limited to eight samples, our training data were biased toward locating these eight samples, even with the inclusion of additional meteorite images acquired from an internet search. Expanding the training data set to include more meteorite images from the internet and more drone-acquired images of meteorites other than the eight we had in our collection would increase the diversity of meteorites in the training data. Every time the drone system is deployed in the field, it generates new data that can later be added to the training data to create a newly trained object detection model. Bringing new meteorites not previously in our collection and deploying them during future field tests would allow for continued improvement of our trained object detection model. This option, however, is limited by the availability of additional meteorites to bring into the field. We also noticed during our tests that the accuracy of the classifier was related to several variables, including the resolution of the training and test images. It is possible that an improved camera resolution or more stable height control could decrease the amount of false positives.

In addition to updating the training data set, we can also improve the object detection network and method of training the final model. For example, we could determine if certain iterations of training data result in more efficient object detection by training RetinaNet with varied training data sets and adjusting factors such as the ratio of images acquired from the internet to images of our collection of eight fragments, image resolution, or the overall size of the training data. We could also test other object detection networks to determine if certain network architectures are more efficient when trained on our data set. Although RetinaNet represents the state of the art in machine learning and is widely used in computer vision and object detection, machine learning is a rapidly evolving field and it is possible that a newer machine learning approach could be even more effective. Future work could more directly compare the effectiveness of various types of object detection networks.

Fig. 5. Example 1000 × 600 pixel image patches from Fig. 4 containing (a) correctly identified meteorites (score = 1.0) that we placed in the test area from our collection and (b) false positives (scores = 0.89 and 0.76). (Color figure can be viewed at wile yonlinelibrary.com.)

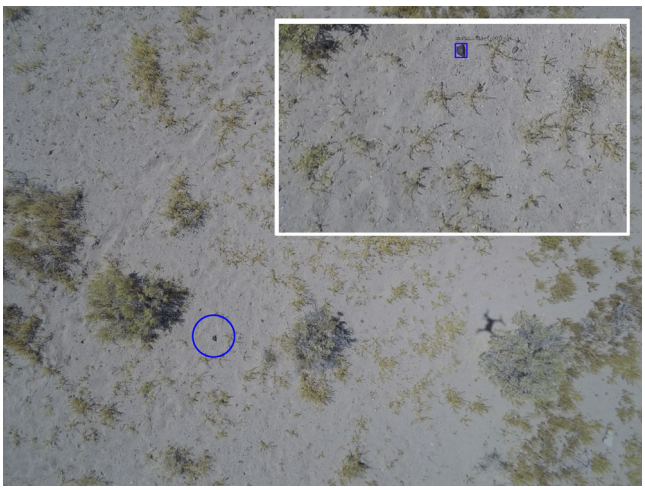

Fig. 6. Example image showing a candidate meteorite identified during the higher altitude field test flights. The large image shows the full 4000 × 3000 pixel GoPro image obtained from the drone, with the candidate meteorite circled in blue. The inset shows the enlarged 1000 × 600 pixel image patch run through the object detection model with the meteorite outlined in a blue box (model score = 1.0). (Color figure can be viewed at wileyonlinelibrary.com.)

It is also unclear how our model performs in varying cloud cover and lighting conditions. The technique as currently developed is intended to operate on clear days when the sun is not too close to the horizon, in order to avoid long shadows that might disrupt the object detection algorithm. The model was trained largely on images of our collection of eight meteorites that were captured in mostly clear conditions so should be most suitable for similar conditions. However, many of the meteorite images obtained from the internet could have been captured in cloudy conditions (although it is difficult to tell from the top-down images without further context), implying that our model could contain some degree of training to detect meteorites in cloudy weather. Cloudy skies would reduce sharp shadows, which could eliminate some false detections; however, the lack of sunlight could also make differentiating various types of rocks more difficult. In particular, the fusion crust on freshly fallen meteorites often has a glassy appearance that is easier to identify in well-lit conditions. In order to expand our model to varying lighting conditions, we could add training images acquired with varied cloud cover into our training data set. We could also artificially decrease or increase the brightness of the training images during data augmentation to introduce more varied lighting conditions into our model.

In addition to improving the machine learning algorithm, our field test identified several hardware improvements necessary to make drone surveys fully effective. We found that surveys at 2 or 3 m covered too small of an area to be particularly efficient. These

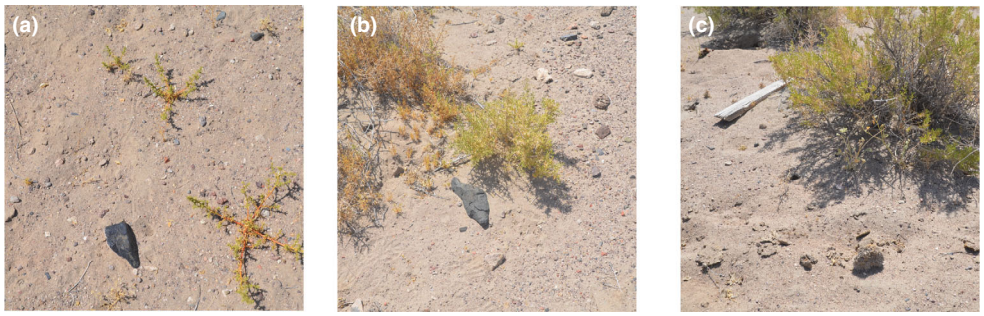

Fig. 7. Images of meteorite candidates taken close-up with a DSLR camera after being geolocated in the field. Panels (a), (b), and (c) correspond to candidates in the drone imagery identified in Figs. 6 and S1 and S2, respectively. (Color figure can be viewed at wileyonlinelibrary.com.)

surveys also located more false positives than the 6 m surveys. However, the GoPro camera is not high enough resolution to be fully effective for surveys conducted at 6 m altitude. Camera wobble also contributed to minor image blur, which made object detection more difficult. Our system therefore requires a drone with an upgraded camera that can take higher resolution photos from 6 m. This is not possible with the 3DR Solo Drone, which can only mount a GoPro camera, meaning a new drone system is required. Unfortunately, there is no economical (<$5000) commercial drone that has a high-resolution camera and can also use a laser altimeter to maintain constant elevation above the ground. However, drone technology is continually being improved, so a new hardware solution that is within reach of regular consumers may present itself in the future.

Overall, the improvements outlined above should decrease the number of false positives detected by our algorithm. As shown in Table 1, many false-positive patches were identified by our object detection classifier, particularly at low survey altitudes of 2–3 m. This implies that our technique is currently limited to the detection of larger meteorites. The biggest improvement may come from better hardware; a higher resolution camera with a more stable gimbal to better dampen camera wobble would increase the resolution and sharpness of each image and improve the likelihood of proper object classification. Augmenting our data set with additional meteorite samples should also increase the accuracy of the object detection network and decrease false positives. Even with these improvements, the application of our technique is likely terrain dependent, as terrains with many dark rocks of similar scale to meteorites may produce an untenable number of false positives regardless of the object detection algorithm or imaging hardware.

Another issue is how to best filter the large number of flagged candidates with models' scores between 0 and 1 to a subset more easily parsed to find the best follow-up candidates. In our field test, we examined all candidates with a score >0.5; however, a higher cutoff value would reduce the time spent searching for follow-up candidates. Because we only tested the model on meteorites used in our training set, it is unclear what model score our algorithm would assign to novel meteorites. Testing our model with field data from additional meteorites not used in the training data could constrain the expected range of scores for new meteorite targets. This would more accurately assess the performance of the machine learning algorithm and help refine future search efforts.

The original intention of the project was to process the images on-site with the object detection classifier so that flagged positives could immediately be closely inspected in situ during the same field trip. However, our field test found this to be ineffective because outdoor lighting conditions made it difficult to scan through images on the laptop in the field. The relatively fast image processing time of ~6 s means that in theory images could be processed at the same rate that they are acquired with drone flights. However, this requires a larger team and more equipment (such as a power source for the laptop) so that one user could run the classifier on the images while another user conducts the next test flight.

Overall, the object detection network deployed in this work presented a major improvement over the direct image classifier used in our previous field test (Citron et al. 2017). Our results showed that the trained RetinaNet object detection network was highly effective on our data set, and could locate meteorites on terrain not used for training the model. RetinaNet reduced the image processing time and increased the accuracy of our model. Although our model still detected many false positives, for 6 m flights, there was a sufficiently low number of positive image patches that a user could scan through the data in a reasonable timeframe and flag

meteorite candidates for follow-up examination. The demonstrated ability to locate flagged meteorites in subsequent field excursions shows that the system can be used to locate freshly fallen meteorites.

CONCLUSIONS

We demonstrated that as a proof of concept, it is possible to identify meteorites in the field by applying an object detection classifier to images acquired with an autonomous drone. As a first step at automating meteorite detection, we constructed a large data set of meteorite images and trained an object detection network. We demonstrated the accuracy of our classifier in the field over terrain not used in our training data set and were able to locate meteorite candidates identified by our classifier during subsequent field trips.

With a larger training data set, updated classification scheme, and improved imaging hardware, machine learning coupled to an autonomous drone survey could prove a valuable tool for increasing the number of meteorites found from fresh falls. This is particularly important for fresh meteorite falls where only small fragments are expected. These falls are unlikely to draw the attention of meteorite hunters, but if the fall is imaged with an all-sky survey, locating fragments is essential to augmenting the number of freshly fallen meteorites with entry orbits computed from imaged fireball trajectories. By constructing a more efficient classifier for locating meteorites in the field, it may be possible to increase the number of meteorites found that can be associated with imaged fireball trajectories, increasing our understanding of the composition of meteors and their parent asteroid bodies.

Acknowledgments—We thank Ilias Fernini and an anonymous reviewer for comments that helped to improve the manuscript and editor Mike Zolensky for handling the manuscript. This project was completed as part of the 2016 NASA Frontier Development Lab, which was supported by the NASA Office of the Chief Technologist. We would like to thank Jason Utas for assistance with our prior Creston, CA, field study. We also thank Fabio Teixeira and Brian Lim of Hypercube and Carlos Uranga for help testing various drone designs. We thank James Parr and Jordan McRae, codirectors of FDL; as well as Jim Adams, deputy chief technologist for NASA; Bruce Pittman, Chief Systems Engineer at NASA Ames Research Center; Bill Diamond, CEO of the SETI Institute; Debbie Kolyer, Grants Manager of the SETI Institute; Jonathan Knowles, explorer in Residence at Autodesk; Alison Lowndes, Deep Learning Solutions for NVIDIA; Eric Dahlstrom, President of the International Space University; Yarin Gal, University of Cambridge Research Fellow. The fieldwork was coordinated with the tribal leaders of the Walker River Northern Paiute Tribe. We thank especially Cheri Clenneding and her interns for assisting in the search. The Global Fireball Observatory is supported by the Australian Research Council. RC and PJ are supported by NASA grant 80NSSC18K0854.

Data Availability Statement—Data used in this study are available on request.

Editorial Handling—Dr. Michael Zolensky

REFERENCES

Abadi M., Agarwal A., Barham P., Brevdo E., Chen Z., Citro C., Corrado G. S., Davis A., Dean J., Devin M., Ghemawat S., Goodfellow I., Harp A., Irving G., Isard M., Jia Y., Jozefowicz R., Kaiser L., Kudlur M., Levenberg J., Mané D., Monga R., Moore S., Murray D., Olah C., Schuster M., Shlens J., Steiner B., Sutskever I., Talwar K., Tucker P., Vanhoucke V., Vasudevan V., Viégas F., Vinyals O., Warden P., Wattenberg M., Wicke M., Yu Y., and Zheng X. 2015. TensorFlow: Large-scale machine learning on heterogeneous systems. tensorflow.org. Accessed May 24, 2020.

Alowais A., Naseem S., Dawdi T., Abdisalam M., Elkalyoubi Y., Adwan A., Hassan K., and Fernini I. 2019. Meteorite hunting using deep learning and UAVs. 2nd International Conference on Signal Processing and Information Security (ICSPIS). pp. 1–4.

Anderson S. L., Bland P. A., Towner M. C., and Paxman J. P. 2019. Utilizing drones and machine learning for meteorite searching and recovery (abstract #2426). 50th Lunar and Planetary Science Conference.

Anderson S., Towner M., Bland P., Haikings C., Volante W., Sansom E., Devillepoix H., Shober P., Hartig B., Cupak M., Jansen-Sturgeon T., Howie R., Benedix G., and Deacon G. 2020. Machine learning for semi-automated meteorite recovery. *Meteoritics & Planetary Science* 55:2461–2471. https://doi.org/10.1111/maps.13593

Borovička J., Spurnỳ P., and Brown P. 2015. Small near-earth asteroids as a source of meteorites. In *Asteroids* edited by Michel P., DeMeo F. E., and Tuscon B. W. F. Tucson, Arizona: University of Arizona Press. https://doi.org/10.2458/azu_uapress_9780816532131-ch014

Chollet F. 2015. Keras: Deep learning library for Theano and TensorFlow. Github Repository.

Citron R. I., Shah A., Sinha S., Watkins C., and Jenniskens P. 2017. Meteorite recovery using an autonomous drone and machine learning (abstract #2528). 48th Lunar and Planetary Science Conference.

Devillepoix H., Cupák M., Bland P. A., Sansom E. K., Towner M. C., Howie R. M., Hartig B., Jansen-Sturgeon T., Shober P. M., Anderson S. l., Benedix G. K., Busan D., Sayers R., Jenniskens P., Albers J., Herd C., Hill P., Brown P. G., Krzeminski Z., Osinski G. R., Aoudjehane H. C., Benkhaldoun Z., Jabiri A., Guennoun M., Barka A., Darhmaoui H., Daly L., Collins G. S., McMullan S., Suttle M. D., Ireland T., Bonning G., Baeza L., Alrefay T.

Y., Horner J., Swindle T. D., Hergenrother C. W., Fries M. D., Tomkins A., Langendam A., Rushmer T., O'Neill C., Janches D., Hormaechea J. l., Shaw C., Young J. S., Alexander M., Mardon A. D., and Tate J. R. 2020. A global fireball observatory. *Planetary and Space Science* 191:105036. https://doi.org/10.1016/j.pss.2020.105036.

Gardiol D., Barghini D., Buzzoni A., Carbognani A., Di Carlo M., Di Martino M., Knapic C., Londero E., Pratesi G., Rasetti S., Riva W., Salerno R., Stirpe G. m., Valsecchi G. B., Volpicelli C. A., Zorba S., Colas F., Zanda B., Bouley S., Jeanne S., Malgoyre A., Birlan M., Blanpain C., Gattacceca J., Lecubin J., Marmo C., Rault J. l., Vaubaillon J., Vernazza P., Affaticati F., Albani M., Andreis A., Ascione G., Avoscan T., Bacci P., Baldini R., Balestrero A., Basso S., Bellitto R., Belluso M., Benna C., Bernardi F., Bertaina M. E., Betti L., Bonino R., Boros K., Bussi A., Carli C., Carriero T., Cascone E., Cattaneo C., Cellino A., Colombetti P., Colombi E., Costa M., Cremonese G., Cricchio D., D'Agostino G., D'Elia M., De Maio M., Demaria P., Di Dato A., Di Luca R., Federici F., Gagliarducci V., Gerardi A., Giuli G., Guidetti D., Interrante G., Lazzarin M., Lera S., Leto G., Licchelli D., Lippolis F., Manca F., Mancuso S., Mannucci F., Masi R., Masiero S., Meucci S., Misiano A., Moggi Cecchi V., Molinari E., Monari J., Montemaggi M., Montesarchio M., Monti G., Morini P., Nastasi A., Pace E., Pardini R., Pavone M., Pegoraro A., Pietronave S., Pisanu T., Pugno N., Repetti U., Rigoni M., Rizzi N., Romeni C., Romeo M., Rubinetti S., Russo P., Salvati F., Selvestrel D., Serra R., Simoncelli C., Smareglia R., Soldi M., Stanga R., Strafella F., Suvieri M., Taricco C., Tigani Sava G., Tombelli M., Trivero P., Umbriaco G., Vairetti R., Valente G., Volpini P., Zagarella R., and Zollo A. 2020. Cavezzo, the first Italian meteorite recovered by the prisma fireball network. Orbit, trajectory, and strewn-field. *Monthly Notices of the Royal Astronomical Society* 501:1215–1227. https://doi.org/10.1093/mnras/staa3646.

Gu J., Wang Z., Kuen J., Ma L., Shahroudy A., Shuai B., Liu T., Wang X., Wang G., Cai J., and Chen T. 2018. Recent advances in convolutional neural networks. *Pattern Recognition* 77:354–377. https://doi.org/10.1016/j.patcog.2017.10.013

He K., Zhang X., Ren S., and Sun J. 2016. Deep residual learning for image recognition. Proceedings of the IEEE Conference on Computer Vision and Pattern Recognition (CVPR). pp. 770–778.

Jenniskens P. 2013. Recent documented meteorite falls, a review of meteorite–asteroid links, Meteoroids 2013. Proceedings of the astronomical conference held at AM University, Poznan. pp. 57–68.

Jenniskens P. 2018. Review of asteroid-family and meteorite-type links. *Proceedings of the International Astronomical Union* 14:9–12.

Jenniskens P., Betlem H., Betlem J., Barifaijo E., Schlüter T., Hampton C., Laubenstein M., Kunz J., and Heusser G. 1994. The Mbale meteorite shower. *Meteoritics* 29:246–254. https://doi.org/10.1111/j.1945-5100.1994.tb00678.x

Jenniskens P., Fries M. D., Yin Q.-Z., Zolensky M., Krot A. N., Sandford S. A., Sears D., Beauford R., Ebel D. S., Friedrich J. M., Nagashima K., Wimpenny J., Yamakawa A., Nishiizumi K., Hamajima Y., Caffee M. W., Welten K. C., Laubenstein M., Davis A. M., Simon S. B., Heck P. R., Young E. D., Kohl I. E., Thiemens M. H., Nunn M. H., Mikouchi T., Hagiya K., Ohsumi K., Cahill T. A., Lawton J. A., Barnes D., Steele A., Rochette P., Verosub K. l., Gattacceca J., Cooper G., Glavin D. P., Burton A. S., Dworkin J. P., Elsila J. E., Pizzarello S., Ogliore R., Schmitt-Kopplin P., Harir M., Hertkorn N., Verchovsky A., Grady M., Nagao K., Okazaki R., Takechi H., Hiroi T., Smith K., Silber E. A., Brown P. G., Albers J., Klotz D., Hankey M., Matson R., Fries J. A., Walker R. J., Puchtel I., Lee C.-T A., Erdman M. E., Eppich G. R., Roeske S., Gabelica Z., Lerche M., Nuevo M., Girten B., and Worden S. P. 2012. Radar-enabled recovery of the Sutter's Mill meteorite, a carbonaceous chondrite regolith breccia. *Science* 338:1583–1587. https://doi.org/10.1126/science.1227163

Jenniskens P., Utas J., Yin Q.-Z., Matson R. D., Fries M., Howell J. A., Free D., Albers J., Devillepoix H., Bland P., Miller A., Verish R., Garvie L. A. J., Zolensky M. E., Ziegler K., Sanborn M. E., Verosub K. L., Rowland D. J., Ostrowski D. R., Bryson K., Laubenstein M., Zhou Q., Li Q.-L., Li X.-H., Liu Y. U., Tang G.-Q., Welten K., Caffee M. W., Meier M. M. M., Plant A. A., Maden C., Busemann H., and Granvik M. 2019. The Creston, California, meteorite fall and the origin of L chondrites. *Meteoritics & Planetary Science* 54:699–720. https://doi.org/10.1111/maps.13235

Jia Y., Shelhamer E., Donahue J., Karayev S., Long J., Girshick R., Guadarrama S., and Darrell T. 2014. Caffe: Convolutional architecture for fast feature embedding. Proceedings of the 22nd ACM international conference on Multimedia. pp. 675–678.

LeCun Y., Bottou L., Bengio Y., and Haffner P. 1998. Gradient-based learning applied to document recognition. *Proceedings of the IEEE* 86:2278–2324.

Lin T. Y., Goyal P., Girshick R., He K., and Dollár P. 2017. Focal loss for dense object detection. Proceedings of the IEEE International Conference on Computer Vision. pp. 2980–2988.

Popova O. P., Jenniskens P., Emel'yanenko V., Kartashova A., Biryukov E., Khaibrakhmanov S., Shuvalov V., Rybnov Y., Dudorov A., Grokhovsky V. I., Badyukov D. D., Yin Q.-Z., Gural P. S., Albers J., Granvik M., Evers L. G., Kuiper J., Kharlamov V., Solovyov A., Rusakov Y. S., Korotkiy S., Serdyuk I., Korochantsev A. v., Larionov M. Y., Glazachev D., Mayer A. E., Gisler G., Gladkovsky S. V., Wimpenny J., Sanborn M. E., Yamakawa A., Verosub K. l., Rowland D. J., Roeske S., Botto N. W., Friedrich J. M., Zolensky M. E., Le L., Ross D., Ziegler K., Nakamura T., Ahn I., Lee J. I., Zhou Q., Li X.-H., Li Q.-l., Liu Y., Tang G.-Q., Hiroi T., Sears D., Weinstein I. A., Vokhmintsev A. S., Ishchenko A. V., Schmitt-Kopplin P., Hertkorn N., Nagao K., Haba M. K., Komatsu M., and Mikouchi T. 2013. Chelyabinsk airburst, damage assessment, meteorite recovery, and characterization. *Science* 342:1069–1073. https://doi.org/10.1126/science.1242642

Russakovsky O., Deng J., Su H., Krause J., Satheesh S., Ma S., Huang Z., Karpathy A., Khosla A., Bernstein M., Berg A. C., and Fei-Fei L. 2015. Imagenet large scale visual recognition challenge. *International Journal of Computer Vision* 115:211–252. https://doi.org/10.1007/s11263-015-0816-y

Zender J., Rudawska R., Koschny D., Drolshagen G., Netjes G. J., Bosch M., Bijl R., Crevecoeur R., and Bettonvil F. 2018. Meteorite detection with airborne support—A study case. Proceedings of the International Meteor Conference. pp. 145–152.

SUPPORTING INFORMATION

Additional supporting information may be found in the online version of this article.

Fig. S1. Example image showing a candidate meteorite identified during the higher altitude field test flights. The large image shows the full 4000 × 3000 pixel GoPro image obtained from the drone, with the candidate meteorite circled in blue. The inset shows the enlarged 1000 × 600 pixel image patch run through the object detection model with the meteorite outlined in a blue box (model score = 0.998).

Fig. S2. Example image showing a candidate meteorite identified during the higher altitude field test flights. The large image shows the full 4000 × 3000 pixel GoPro image obtained from the drone, with the candidate meteorite circled in blue. The inset shows the enlarged 1000 × 600 pixel image patch run through the object detection model with the meteorite outlined in a blue box (model score = 0.992).